Anisotropic Encapsulation-Induced Synthesis of Asymmetric Single-Hole Mesoporous Nanocages

Xiaomin Li,[†] Lei Zhou,[†] Yong Wei,[†] Ahmed Mohamed El-Toni,[‡,§] Fan Zhang,*[,†] and Dongyuan Zhao*[,†]

[†]Laboratory of Advanced Materials, Department of Chemistry, State Key Laboratory of Molecular Engineering of Polymers and iChEM (Collaborative Innovation Center of Chemistry for Energy Materials), Fudan University, Shanghai 200433, P. R. China
[‡]King Abdullah Institute for Nanotechnology, King Saud University, Riyadh 11451, Saudi Arabia
[§]Central Metallurgical Research and Development Institute, CMRDI, Helwan 11421, Cairo, Egypt

S *Supporting Information*

ABSTRACT: Asymmetric single-hole mesoporous silica nanocages, which are eccentric hollow structured spheres and consist of mesoporous shell with an open hole on their surface, with uniform particle size (100−240 nm), have successfully been synthesized via a novel anisotropic encapsulation of the mesoporous silica. In this unique nanocarrier, the eccentric hollow cavity and big hole (∼25 nm) can serve as a storage space and passage for large guest molecules. Meanwhile, the uniform mesopores (2−10 nm) with a high surface area (∼500 m^2/g) in the silica shells of the nanocages can provide storage space for small guest molecules. The obtained single-hole mesoporous nanocages can be endowed upconversion luminescence. The obtained upconversion nanoparticles functionalized eccentric single-hole nanorattles were used to codeliver bovine serum albumin and doxorubicin dual-sized guests. The release of the dual-sized guests can be well controlled independently by heat and near-infrared (NIR) light with the assistance of NIR to ultraviolet/visible (UV/vis) optical properties of upconversion nanoparticles and heat-sensitive phase change materials.

During the past decades, mesoporous colloidal nanoparticles with hollow interiors play important roles in nano-encapsulation, a process that has found widespread use in controlled release of drugs, cosmetics, inks, pigments, or chemical reagents; protection of biologically active species; and removal of pollutants.[1−6] However, the diameter of the guest molecules loaded in the hollow nanoparticles is quite restricted by the pore size of closed shells, especially for the large entities such as proteins, enzymes, etc.

The cage-structured particles with a single hole in the shells, referred to as single-hole nanocages, have stimulated significant interest because of their highly effective diffusivity, large available surface area, and up-taking capacity for big guest molecules. The guest molecules can diffuse in or out of the nanocages easily because of the big hole in the shells. However, the single-hole caged particles reported previously, such as polystyrene (PS),[7,8] poly(methylsilsesquioxane),[9] poly(acryamide-ethylene glycol dimethacrylate),[10] PS/poly(divinylbenzene),[11] and PS/poly-(3,4-ethylenedioxythiophene),[12] are often close to micrometer in size and typically involved various types of toxic organic polymers. Mesoporous silica nanoparticles are considered to be

one of the most popular materials for the design of the drug delivery systems because of their high biocompatibility, large surface area, ease of functionalization, etc.[13−15] However, the mesoporous silica nanoparticles are often widely used for building symmetrical concentric structures, such as nano-spheres,[16−18] hollow nanospheres,[19−21] yolk−shell nano-spheres,[22−24] etc. The fabrication of asymmetrical eccentric mesoporous silica nanocage with a transverse big hole on its surface remains a challenge, partly because of the lack of growth approach enabling pore structure control in different compart-ments of the same particle. Identifying such growth mechanism would enable access to locally amorphous, mesoscopically ordered nanoparticles with a high degree of architectural complexity yet highly controlled shapes and assemblies.

Herein, we report an anisotropic encapsulation method for the synthesis of the asymmetrical eccentric single-hole mesoporous silica nanocages. The new anisotropic encapsulation can yield unique asymmetrical eccentric mesoporous nanocages with uniform particle size (100−240 nm). The diameters of the hollow voids can well be controlled (35−170 nm). In the asymmetric single-hole nanocages, the hollow cavity with a big hole can serve as a storage space with a passage for large guests, respectively. Meanwhile, the mesopore shells (3−10 nm) with a high BET surface area (∼500 m^2/g) of the eccentric nano-particles with hollow cages and mesopores can also serve as a storage space and channel for the small molecules. The obtained single-hole mesoporous nanocages can be further functionalized with upconversion nanoparticles (UCNPs). By using doxor-ubicin (DOX, <1 nm^3) and albumin from bovine serum (BSA, 21 × 4 × 14 nm^3) as model guests, the obtained UCNPs-functionalized eccentric single-hole nanocages were used as a nanocarrier for dual-sized guests codelivery system with the high loading capacities of 342 and 33.6 mg/g for BSA and DOX, respectively. The release of dual-sized guests can be well controlled independently by heat and NIR light with the assistance of the NIR to UV/vis optical property of UCNPs and heat-sensitive phase change materials.

The eccentric single-hole mesoporous nanocages can be synthesized through three steps (Figure 1A): anisotropic encapsulation, hydrothermal treatment, and HF etching. Dense SiO$_2$ spherical nanoparticles with a uniform particle size (35−
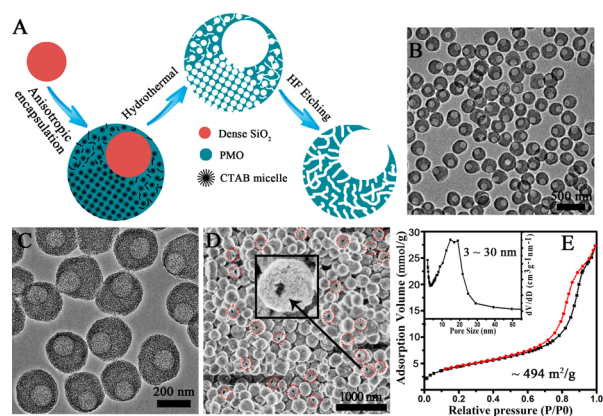
Figure 1. (A) Synthetic procedure for the asymmetric single-hole mesoporous nanocages. (B,C) TEM and (D) SEM images of the obtained asymmetric single-hole mesoporous nanocages. (E) N_2 sorption isotherms and the pore size distribution of single-hole mesoporous nanocages.

170 nm) could be used as an initial seed (Figure S1). By using the hexadecyltrimethylammonium bromide (CTAB) as a meso-structural template and 1,2-bis(triethoxysilyl) ethane (BTEE) as a silica precursor, periodic mesoporous organosilica (PMO) could be nucleated[25] and anisotropically encapsulated on the dense SiO_2 nanoparticles to form the eccentric SiO_2@PMO core@shell nanocomposites (Figures S2 and S3A). After the hydrothermal treatment at 60 °C for 12 h, the dense SiO_2 nanoparticles could be etched, and the eccentric hollow PMO nanoparticles were formed (Figure S4). In this step, the shells of the eccentric hollow PMO nanoparticles were closed. Finally, HF solution was used to etch the hollow PMO nanoparticles. Because of the eccentric structure of the hollow PMO nanoparticles, the single hole could appear at the thinner side of the PMO shells during the etching process to realize the eccentric hollow PMOs with an open hole on the shells (Figure 1B−D).

Transmission electron microscopy (TEM) images (Figure 1B,C) of the obtained nanoparticles clearly show an eccentric caged nanostructure with a uniform particle size of ∼220 nm. The diameter of the hollow cages is about 120 nm, which is consistent with the size of the initial SiO_2 seeds. After HF etching, the ordered PMOs frameworks were degenerated, showing a disordered worm-like mesopore in the shells. Statistical result shows that the diameter of the mesopore channels is about 2−10 nm. Scanning electron microscopy (SEM) image of the single-hole mesoporous nanocages (Figure 1D) shows that the silica shell is open, and it possesses only a single hole with an opening of ∼25 nm on the surface of each particle. N_2 sorption isotherms of the obtained single-hole mesoporous nanocages (Figure 1E) exhibit typical type-IV curves with a rapid increase in the adsorption branch at a relative pressure of 0.7−0.9, indicating that the nanocages contain very open mesopore channels. The BET surface area is ∼494 m^2/g. The broad pore size distribution in the range of 3−30 nm (Figure 1E) can be attributed to the disordered mesoporous shell and the single hole. By tuning the amount of the silane precursor, the size of the dense SiO_2 seeds and HF etching time, the diameters of the nanocages, hollow cavity, and the single-hole can be well controlled at 100−240, 35−170, and 10−40 nm (Figures S6 and S7).

Owing to HF resistance of $NaGdF_4$, the eccentric single-hole mesoporous nanocages can be further imbued with upconversion luminescence (denoted as single-hole UCNP@MSN nano-

rattles) by using UCNP@SiO_2 as the initial seed. The monodispersed $NaGdF_4$:25%Yb,0.5%Tm@$NaGdF_4$ upconversion nanodisks with a size of ∼35 nm were synthesized by using the well established method.[26,27] Afterward, a dense silica layer was coated on UCNP to form the UCNP@SiO_2 nanoparticles (Figure S9). TEM images (Figures 2A and S10) of the obtained
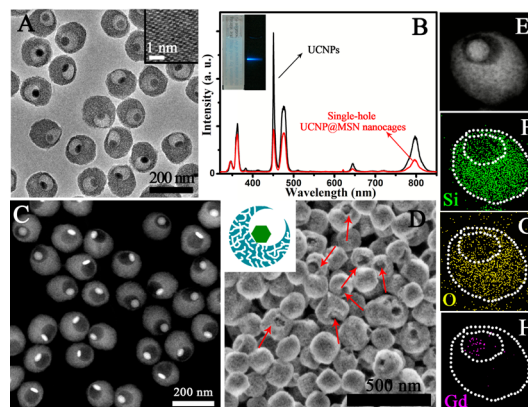

Figure 2. (A) TEM image of the obtained eccentric single-hole UCNP@MSN nanorattles. (B) The upconversion luminescence spectra of the $NaGdF_4$:Yb,Tm@$NaGdF_4$ UCNPs and single-hole UCNP@MSN nanorattles. (C,D) HAADF-STEM and SEM images of the single-hole nanorattles. (E−H) Element mapping of Si, O, and Gd elements in one single-hole nanorattle.

single-hole nanorattles show a uniform spherical shape with an average diameter of ∼150 nm. The nanorattles retain the morphology of the hollow structure with a single hole on the surface of the shell and a UCNP in one cage (Figure 2C,D). In addition, the single-hole nanorattles can also exhibit unique NIR-to-UV/vis upconversion optical property (Figure 2B). Elemental mapping shows that all the expected elements, including silicon and oxygen, and gadolinium elements can be detected and matched well with the relative positions in the single-hole UCNP@MSN nanorattles (Figure 2E−H).

It has been demonstrated that the mesostructures can be oriented by surfactant micelles and further induced the anisotropic growth for the mesoporous silica shells on the surface.[25,28] Owing to the anisotropic growth of the mesostructure, various nanomaterials with eccentric morphology can be synthesized, such as Janus nanocomposites,[25] multipodal PMOs,[29] branched mesoporous silica nanoparticles,[28] and so on. To the best of our knowledge, this is the first report on the synthesis of eccentric single-hole mesoporous silica nanocages. The shape evolution of the obtained single-hole mesoporous nanocages (Figures 3A−C, S2, and S3) show that the asymmetric Janus mesoporous nanostructures were formed at the early stage of the PMO growth process (Figure 3A,D). As the reaction prolongs, the SiO_2 nanoparticles were continuously wrapped by the cubic PMO crystals, the exposed portion of the SiO_2 seeds was gradually decreased (Figures 3B, S2B, and S2C) until it disappeared (all covered by PMO crystals). Finally, the eccentric SiO_2@PMO core@shell nanocomposites were obtained. It can be seen that the morphology of the PMO domains was changed from cubic to near-spherical. The fast Fourier transform results of the Janus (Figure 3D), eccentric SiO_2@PMO core@shell, and eccentric hollow structured nanoparticles (Figure 3E) show that the PMO domain can be divided into the ordered region (marked with green) and disordered region (marked with blue). The proportion of the disordered region in the PMO domain
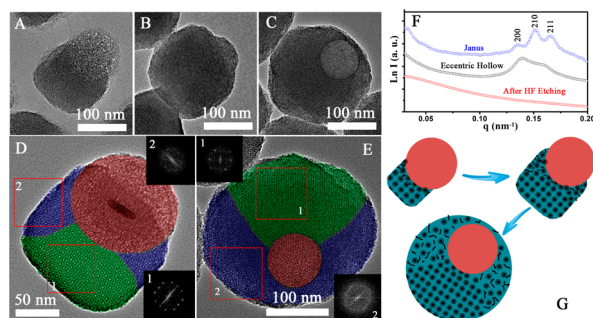
Figure 3. TEM images (A−C) of the morphology evolution of the eccentric nanocomposites. (D,E) TEM images of the obtained Janus UCNPs@SiO$_2$ and PMO and the eccentric hollow structured nanocomposites. Inset is the corresponding fast Fourier transform of the area marked with the red square. (F) The SAXS pattern of the Janus, eccentric hollow nanocomposites, and the single-hole mesoporous nanocages after the HF etching. (G) The growth evolution of PMO domain on the SiO$_2$ nanoparticles.

gradually increases during the encapsulation process, which is consistent with small-angle X-ray scattering (SAXS) patterns (Figure 3F). On the basis of the aforementioned results, we believe that the successful synthesis of the eccentric single-hole mesoporous nanocages experiences three stages: anisotropic nucleation, anisotropic growth, and the anisotropic encapsulation (Figure 3G). Because of the distinct chemical properties between TEOS and BTEE, the latter precursor leans toward anisotropic polymerization on the surface of the dense SiO$_2$ seeds through a heterogeneous nucleation process.[25] The negative total surface energy variation ($\triangle\sigma = \sigma_{PMO-solvent} + \sigma_{PMO-SiO2} - \sigma_{SiO2-solvent} < 0$) and the cubic symmetry mesostructure of the PMO domains (Figure S5) could further induce the formation of the Janus nanostructure (see the Supporting Information for the details). It is worth mentioning that the "lattice" mismatch between the dense SiO$_2$ (nonporous) and PMO (cubic symmetry mesostructure) can induce the formation of disordered region at the heterointerface. The growth of this disordered region is synchronized with the ordered cubic mesostructured region. As the PMO domains are continuously wrapping and growing, the cubic symmetry PMO crystals enlarge and the heterointerface increases. So, the ratio of the disordered region in the eccentric SiO$_2$@PMO core@shell nanocomposites increases. Owing to the presence of the great amount of disordered mesostructural defects in the final products, the morphology of the PMO domains were transferred from cubic to the near-spherical, for further lowering the interface tension. Therefore, the whole dense SiO$_2$ nanosphere can be covered by the near-spherical PMO shells, the eccentric core@shell nanoparticles are formed.

The unique big single-hole, cage, and abundant mesopore shells promise the eccentric single-hole mesoporous nanocage to be a good nanocarrier for dual-sized guest codelivery. The cytotoxicity of this nanocarrier (Figure 4A) shows that the viability of the cells is maintained more than 95% even at a high concentration (∼100 μg/mL), indicating a good biocompatibility of the nanocarrier. In this nanocarrier, there are dual independent storage spaces for guest molecules. One is the hollow cave for big guest molecules, another is the mesopores in the PMO shells for small guest molecules. Here, we selected two commonly used molecules with quite different sizes, doxorubicin (DOX, <1 nm^3) and albumin from bovine serum (BSA, 21 × 4 × 14 nm^3), as model guests to evaluate potentials of the eccentric
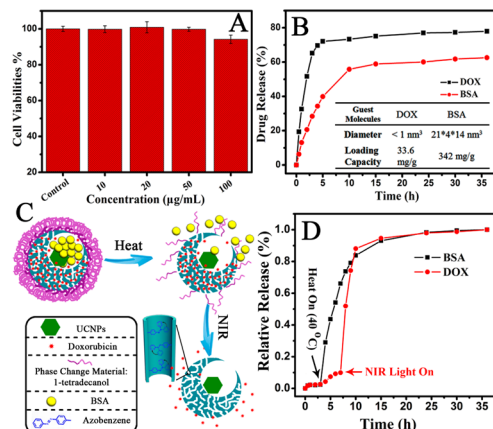

Figure 4. (A) Cell viability assay of the eccentric single-hole UCNP@MSN nanorattles. (B) Free release profiles of bare DOX or BSA molecules from the eccentric single-hole nanorattles. (C) Scheme for controlled release of dual-sized guests by using the single-hole UCNP@MSN nanorattles. (D) Release profiles of DOX and BSA molecules from single-hole nanorattles under the stimuli of heat and NIR light.

single-hole hollow mesoporous silica for the dual-sized guests codelivery system. The loading capacities for BSA and DOX are 342 and 33.6 mg/g, respectively. Figure 4B shows the free release (without the modification of the switch molecules) profiles of bare DOX or BSA molecules from the nanocarrier. The release of small DOX molecules can reach equilibrium in 5 h, which is much faster than that of big BSA molecules (∼15 h). We consider that this discernible variation in release properties results from the different storage spaces for the dual-sized guest molecules.

As a proof of concept, the eccentric single-hole UCNP@MSN nanorattles were further applied for heat and NIR light triggered controllable release of dual-sized guests (BSA and DOX).[7,32] Compared with the traditional dual-pore nanorattles with closed shells,[30,31] the single-hole mesoporous nanocages can provide dual independent storage spaces and releasing channels for the guests with different sizes. As shown in Figure 4C, the single-hole nanorattles were modified with light sensitive azobenzene (Azo) molecules in the mesopore shell channels and heat-sensitive phase change materials (PCM) 1-tetradecanol on the outer surface of the nanoparticles (the obtained nanocomposites are denoted as UCNP@MSN-Azo-PCM) (Figures S14−S16). Below its melting point, PCM is in a solid state to completely block the passing of encapsulated BSA. When the temperature is raised beyond its melting point (38−39 °C), PCM can quickly melt to release the encapsulated BSA in hollow cave passing the big hole.[7] For the NIR-to-UV/vis upconversion luminescence of sensitive Azo molecules, it can transform into cis-isomer from the trans-isomer under UV irradiation (∼360 nm), and in contrast, cis-isomer can convert into trans-isomer under irradiation of visible light (∼450 nm). Upon absorption of NIR light (980 nm), the UCNPs emit photons in the UV/vis region (Figure 2B), which can be absorbed immediately by the photoresponsive Azo molecules in the mesopore shells of the eccentric single-hole nanorattles (Figure S15). The reversible photoisomerization by simultaneous UV and visible light emitted by the UCNPs creates a continuous rotation−inversion movement. The back and forth wagging motions of the Azo molecules act as a molecular impeller that propels the release of encapsulated DOX in the mesopore shells.[32]

The results of this dual-sized guest delivery system show that the negligible releasing of the guest molecules is observed in the

absence of stimuli of the switches (beginning 3 h, Figure 4D). In contrast, the dual-sized guests loaded with nanocomposites upon the heat treatment (~40 °C) show a significantly releasing of BSA molecules in the hollow cave (from 3 to 35 h, Figure 4D) because of the opening of the first switch (PCM). At the same time, only a very small amount of DOX molecules can be detected upon the heat treatment (from 3 to 7 h, Figure 4D). When heat and NIR light are introduced at the same time, both of the switches are triggered to open. The BSA in hollow cave and DOX in the mesopore shells can be released at the same time (from 7 to 35 h, Figure 4D).

In summary, asymmetric eccentric single-hole mesoporous silica nanocages with a very uniform size have successfully been synthesized via the anisotropic encapsulation route, which is featured with simplicity, easy scale-up, and versatility in engineering the architecture of asymmetric nanomaterials. In the obtained unique single-hole nanocages, the hollow cavity and big hole (~25 nm) can serve as a storage space and passage for the large guests. Meanwhile, the mesopores (2−10 nm) with a high surface area (~500 m^2/g) in the silica shells of the hollow particles can provide storage space for the small guests. The obtained single-hole nanocages can also be endowed upconversion luminescence. The obtained eccentric single-hole UCNP@MSN nanorattles can be used as a dual-sized guest (BSA and DOX) codelivery system. The release of the dual-sized guests can be well controlled independently by heat and NIR light. We envision this discovery of the single-hole mesoporous nanocages may lead to further development of new concepts and architectures of nanocarriers, thus allowing for more opportunities in multidrug delivery and combined therapy.

■ ASSOCIATED CONTENT

Ⓢ Supporting Information

Experimental section and additional data. The Supporting Information is available free of charge on the ACS Publications website at DOI: 10.1021/jacs.5b03207.

■ AUTHOR INFORMATION

Corresponding Authors
*zhang_fan@fudan.edu.cn
*dyzhao@fudan.edu.cnz

Notes
The authors declare no competing financial interest.

■ ACKNOWLEDGMENTS

■ REFERENCES

(1) Chen, Y.; Xu, P.; Chen, H.; Li, Y.; Bu, W.; Shu, Z.; Li, Y.; Zhang, J.; Zhang, L.; Pan, L.; Cui, X.; Hua, Z.; Wang, J.; Zhang, L.; Shi, J. *Adv. Mater.* **2013**, *25*, 3100.

(2) Dergunov, S.; Durbin, J.; Pattanaik, S.; Pinkhassik, E. *J. Am. Chem. Soc.* **2014**, *136*, 2212.

(3) Cao, B. R.; Yang, M. Y.; Zhu, Y.; Qu, X. W.; Mao, C. B. *Adv. Mater.* **2014**, *26*, 4627.

(4) Zhang, G. Q.; Wu, H. B.; Song, T.; Paik, U.; Lou, X. W. *Angew. Chem., Int. Ed.* **2014**, *53*, 12590.

(5) Lou, X. W.; Archer, L. A.; Yang, Z. C. *Adv. Mater.* **2008**, *20*, 3987.

(6) Gao, X. H.; Wu, H. B.; Zheng, L. X.; Zhong, Y. J.; Hu, Y.; Lou, X. W. *Angew. Chem. Int. Ed.* **2014**, *53*, 5917.

(7) Hyun, D. C.; Lu, P.; Choi, S. I.; Jeong, U.; Xia, Y. *Angew. Chem., Int. Ed.* **2013**, *52*, 10468.

(8) Im, S. H.; Jeong, U.; Xia, Y. *Nat. Mater.* **2005**, *4*, 671.

(9) Chang, M. W.; Stride, E.; Edirisinghe, M. *Langmuir* **2010**, *26*, 5115.

(10) Guan, G.; Zhang, Z.; Wang, Z.; Liu, B.; Gao, D.; Xie, C. *Adv. Mater.* **2007**, *19*, 2370.

(11) Minami, H.; Kobayashi, H.; Okubo, M. *Langmuir* **2005**, *21*, 5655.

(12) Luo, S. C.; Jiang, J.; Liour, S. S.; Gao, S.; Ying, J. Y.; Yu, H. H. *Chem. Commun.* **2009**, 2664.

(13) Xing, L.; Zheng, H.; Cao, Y.; Che, S. *Adv. Mater.* **2012**, *24*, 6433.

(14) Qian, R.; Ding, L.; Ju, H. *J. Am. Chem. Soc.* **2013**, *135*, 13282.

(15) Zhang, J.; Yuan, Z. F.; Wang, Y.; Chen, W. H.; Luo, G. F.; Cheng, S. X.; Zhuo, R. X.; Zhang, X. Z. *J. Am. Chem. Soc.* **2013**, *135*, 5068.

(16) Shen, D.; Yang, J.; Li, X.; Zhou, L.; Zhang, R.; Li, W.; Chen, L.; Wang, R.; Zhang, F.; Zhao, D. Y. *Nano Lett.* **2014**, *14*, 923.

(17) Du, X.; Shi, B.; Liang, J.; Bi, J.; Dai, S.; Qiao, S. Z. *Adv. Mater.* **2013**, *25*, 5981.

(18) Liu, R.; Zhang, Y.; Zhao, X.; Agarwal, A.; Mueller, L. J.; Feng, P. Y. *J. Am. Chem. Soc.* **2010**, *132*, 1500.

(19) Zhao, Y.; Lin, L. N.; Lu, Y.; Chen, S. F.; Dong, L.; Yu, S. H. *Adv. Mater.* **2010**, *22*, 5255.

(20) Fu, J.; Chen, T.; Wang, M.; Yang, N.; Li, S.; Wang, Y.; Liu, X. *ACS Nano* **2013**, *7*, 11397.

(21) Liu, Y. D.; Goebl, J.; Yin, Y. D. *Chem. Soc. Rev.* **2013**, *42*, 2610.

(22) Fang, Y.; Zheng, G.; Yang, J.; Tang, H.; Zhang, Y.; Kong, B.; Lv, Y.; Xu, C.; Asiri, A. M.; Zi, J.; Zhang, F.; Zhao, D. Y. *Angew. Chem., Int. Ed.* **2014**, *53*, 5366.

(23) Zhu, Y.; Ikoma, T.; Hanagata, N.; Kaskel, S. *Small* **2010**, *6*, 471.

(24) Zhang, T. R.; Ge, J. P.; Hu, Y. X.; Zhang, Q.; Aloni, S.; Yin, Y. D. *Angew. Chem., Int. Ed.* **2008**, *47*, 5806.

(25) Li, X.; Zhou, L.; Wei, Y.; El-Toni, A. M.; Zhang, F.; Zhao, D. Y. *J. Am. Chem. Soc.* **2014**, *136*, 15086.

(26) Li, X.; Shen, D.; Yang, J.; Yao, C.; Che, R.; Zhang, F.; Zhao, D. Y. *Chem. Mater.* **2013**, *25*, 106.

(27) Li, X.; Wang, R.; Zhang, F.; Zhao, D. Y. *Nano Lett.* **2014**, *14*, 3634.

(28) Suteewong, T.; Sai, H.; Hovden, R.; Muller, D.; Bradbury, M. S.; Gruner, S. M.; Wiesner, U. *Science* **2013**, *340*, 337.

(29) Croissant, J.; Cattoen, X.; Man, M. W. C.; Dieudonne, P.; Charnay, C.; Raehm, L.; Durand, J. O. *Adv. Mater.* **2015**, *27*, 145.

(30) Liu, J.; Qiao, S. Z.; Hartono, S. B.; Lu, G. Q. *Angew. Chem., Int. Ed.* **2010**, *49*, 4981.

(31) Fang, Y.; Zheng, G.; Yang, J.; Tang, H.; Zhang, Y.; Kong, B.; Lv, Y.; Xu, C.; Asiri, A. M.; Zi, J.; Zhang, F.; Zhao, D. Y. *Angew. Chem., Int. Ed.* **2014**, *53*, 5366.

(32) Liu, J.; Bu, W.; Pan, L.; Shi, J. *Angew. Chem., Int. Ed.* **2013**, *52*, 4375.